chemosensors

MDPI

Article

Efficient and Selective Multiple Ion Chemosensor by Novel Near-Infrared Sensitive Symmetrical Squaraine Dye Probe

Sushma Thapa, Kshitij RB Singh and Shyam S. Pandey *

Graduate School of Life Science and System Engineering, Kyushu Institute of Technology, 2-4, Hibikino, Wakamatsu, Kitakyushu 808-0196, Japan; sushmathapa858@gmail.com (S.T.); krbs09@gmail.com (K.R.S.)
* Correspondence: shyam@life.kyutech.ac.jp

Abstract

A novel near-infrared (NIR) squaraine-based chemosensor, **SQ-68**, has been designed and synthesized for the sensitive and selective detection of Cu^{2+} and Ag^{+} ions, offering a compact solution for multi-analyte sensing. **SQ-68** demonstrates high selectivity, with its performance influenced by the solvent environment: It selectively detects Cu^{2+} in acetonitrile and Ag^{+} in an ethanol–water mixture. Upon binding with either ion, **SQ-68** undergoes significant absorption changes in the NIR region, accompanied by visible color changes, enabling naked-eye detection. Spectroscopic studies confirm a 1:1 binding stoichiometry with both Cu^{2+} and Ag^{+}, accompanied by hypochromism. The detection limits are 0.09 μM for Cu^{2+} and 0.38 μM for Ag^{+}, supporting highly sensitive quantification. The sensor's practical applicability was validated in real water samples (sea, lake, and tap water), with recovery rates ranging from 73–95% for Cu^{2+} to 59–99% for Ag^{+}. These results establish **SQ-68** as a reliable and efficient chemosensor for environmental monitoring and water quality assessment. Its dual-analyte capability, solvent-tunable selectivity, and visual detection features make it a promising tool for rapid and accurate detection of heavy metal ions in diverse aqueous environments.

Keywords: squaraine dye; chemosensor; metal ion; selective multi-ion sensing; naked eye detection

check for updates

Received: 28 June 2025
Revised: 1 August 2025
Accepted: 1 August 2025
Published: 4 August 2025

Citation: Thapa, S.; Singh, K.R.; Pandey, S.S. Efficient and Selective Multiple Ion Chemosensor by Novel Near-Infrared Sensitive Symmetrical Squaraine Dye Probe. *Chemosensors* **2025**, *13*, 288. https://doi.org/10.3390/chemosensors13080288

Copyright: © 2025 by the authors. Licensee MDPI, Basel, Switzerland. This article is an open access article distributed under the terms and conditions of the Creative Commons Attribution (CC BY) license (https://creativecommons.org/licenses/by/4.0/).

1. Introduction

Squaraine dyes represent a distinct class of near-infrared (NIR) chromophores characterized by a planar, resonance-stabilized zwitterionic structure. These dyes feature a strongly electron-deficient squaric acid core symmetrically conjugated with electron-rich aromatic donor groups, forming a donor–acceptor–donor architecture. This configuration facilitates intense intramolecular charge transfer, resulting in sharp and intense absorption and emission bands in the NIR region (650–900 nm) with high molar absorptivity and photostability [1,2]. Unlike conventional visible–light sensitive dyes, squaraine dyes offer exceptional advantages for sensing applications, including minimal autofluorescence, reduced light scattering, and deep tissue penetration, making them highly suitable for biological sensing applications. Their tunable optical properties, achieved through structural modifications of donor groups or the central squarate ring, make them ideal candidates for designing molecular probes capable of selective ion recognition in complex environments [3,4].

Heavy metal ions such as copper (Cu^{2+}) and silver (Ag^{+}) are critical in numerous biological systems and contribute to various physiological processes, but they pose significant environmental and health risks at elevated concentrations [5–7]. Cu^{2+}, the third

most abundant essential transition metal, is indispensable in enzymatic redox processes, yet its dysregulations are linked to neurodegenerative disorders (e.g., Alzheimer's and Wilson's diseases) and renal dysfunction. The United States Environmental Protection Agency (USEPA) mandates a maximum permissible Cu^{2+} level of 1.3 mg/L in drinking water [8,9]. Similarly, Ag^{+}, widely utilized for its antimicrobial properties in medical and industrial sectors, can cause argyria, organ damage, and growth retardation upon excessive exposure, with a USEPA safety threshold of 0.1 mg/L in drinking water [6,10,11]. Given these concerns, there is a pressing need for the development of a reliable, selective, and portable chemosensor capable of detecting trace levels of Cu^{2+} and Ag^{+} ions. Traditional analytical methods used for the trace determination of ions offer high sensitivity but suffer from limitations, including costly instrumentation and a lack of real-time, on-site applicability. These constraints highlight the need for innovative sensing platforms that combine affordability, user-friendliness, and adaptability across diverse environments. Colorimetric and fluorescent chemosensors have emerged as attractive alternatives due to their simplicity, low cost, and ability to provide real-time, visual detection. These sensors offer several key advantages, including ease of operation, high selectivity, low detection limits, and portability. These features make them particularly suitable for environmental monitoring and point-of-care applications [12–14].

Despite their advantages, most squaraine-based chemosensors reported to date are designed for the recognition of a single analyte and are often tested in a limited solvent environment, such as purely aqueous or organic phases. A multiple ion sensing probe can enhance detection efficiency and save a substantial amount of time and money spent on the synthesis of the probe. To date, there have been many reports on dual-signal probes. However, dual-site probes capable of simultaneously detecting Cu^{2+} and Ag^{+} remain rare. Therefore, designing a squaraine-based NIR chemosensor capable of dual-ion recognition of Cu^{2+} and Ag^{+} and evaluating its sensing performance across multiple solvent systems would provide valuable insights into ion–probe–solvent interactions and broaden the scope of practical deployment. In this study, we present the design, synthesis, and characterization of an NIR-sensitive symmetrical squaraine dye chemosensor, **SQ-68**, developed for the selective and sensitive detection of both Cu^{2+} and Ag^{+} ions in the acetonitrile and ethanol/water solvent systems, respectively. The probe demonstrates high selectivity, low detection limits, and rapid responses in both solvent systems, providing valuable insight into metal–probe–solvent interactions. This work not only advances the development of multifunctional NIR sensors but also provides critical insights into the design of adaptable probes for real-world environmental applications.

2. Experimental Section

2.1. Materials and Instrumentation

The details regarding the instrumentation, reagent specifications, and computational methodologies are comprehensively described in Section S1 of the Supplementary Information. Furthermore, all chemicals applied in this work were of high-purity analytical grade and used as received.

2.2. Synthesis of **SQ-68** *and Dye Intermediates*

The synthesis of the **SQ-68** dye was successfully carried out in six steps, following a previously reported method with certain modifications. The detailed synthetic procedure, including all intermediate compounds, is outlined in Scheme S1 and elaborated in Section S3 of the Supplementary Information (SI) [15]. The structure and purity of synthesized intermediates and the final **SQ-68** dye were confirmed by mass spectrometry (Figures S1–S6) and NMR analysis (Figures S7–S12).

3. Results

3.1. Physicochemical Properties of **SQ-68**

The **SQ-68** was examined physically using UV–vis absorption and fluorescence emission in two different solvent systems—acetonitrile and ethanol: water (1:1, *v*/*v*). Figure 1 illustrates the absorption and emission spectra, while Table 1 summarizes the optical parameters of **SQ-68** in different solvents. In acetonitrile, **SQ-68** exhibited a sharp and intense absorption maximum at 672 nm (Figure 1a) with a high molar extinction coefficient of 2.77 × 10^5 L mol^{-1} cm^{-1}, characteristics of π-π* transitions associated with its monomeric form. In addition to their characteristics, π-π* absorption bands often display a vibronic shoulder in their absorption spectra. When this vibronic shoulder becomes more pronounced and evolves into a distinct secondary peak, it is widely recognized as a spectroscopic indication of molecular aggregation, particularly the formation of H-aggregates [16,17].

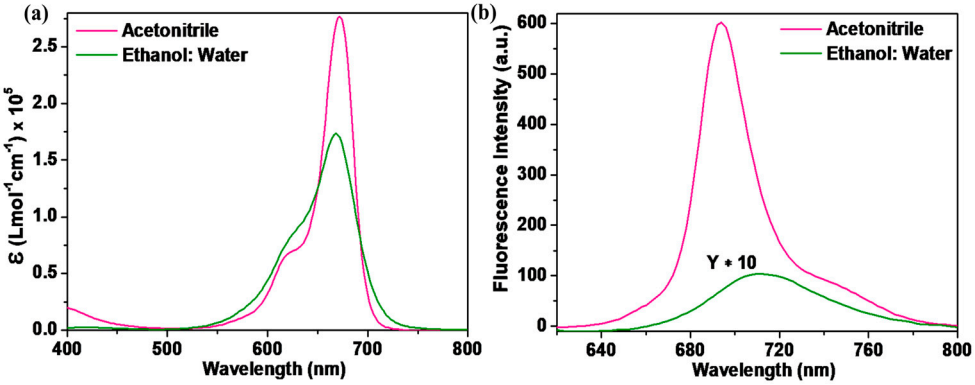


Figure 1. (**a**) Electronic absorption and (**b**) fluorescence emission spectra (λ_{ex} = 610 nm, excitation and emission bandwidths are 5 and 6, respectively) of **SQ-68** (10 μM) in acetonitrile and ethanol: water (1:1, *v*/*v*) mixture.

Table 1. Optical characterization of **SQ-68** in acetonitrile and ethanol: water (1:1, *v*/*v*) solvent system.

Solvent	λ_{abs} (nm)	λ_{emi} (nm)	Stokes Shift (cm^{-1})	Molar Extinction Coefficient (ε) × 10^5 L mol^{-1} cm^{-1}
CH_3CN	672	694	472	2.77
EtOH: H_2O (1:1, *v*/*v*)	670	710	840	1.52

Conversely, when using an ethanol: water (1:1, *v*/*v*) binary solvent mixture, the absorption peak exhibited a slight blue shift to 670 nm (Figure 1b), accompanied by a notable decrease in absorbance. Additionally, the absorption peak exhibited spectral broadening, which is indicative of the formation of aggregates. Such spectral broadening and intensity reduction are commonly observed in squaraine dyes due to their strong tendency to form H-aggregates in polar protic solvents, particularly in aqueous solutions [18,19]. The corresponding emission spectra, as shown in Figure 1b, further corroborate the solvent-dependent behavior of **SQ-68**. In acetonitrile, **SQ-68** shows a strong emission band at 694 nm with a high fluorescence intensity, consistent with an emissive, monomeric state. However, in the ethanol: water (1:1, *v*/*v*) system, a bathochromic shift in the emission maximum was observed at 710 nm, accompanied by a drastic decrease in fluorescence intensity. This pronounced fluorescence quenching is attributed to aggregation-induced non-radiative decay pathways, which are typical for squaraine dyes in aqueous media. To further investigate the solvatochromic behavior of the synthesized **SQ-68**, UV–visible absorption and fluorescence emission spectra were recorded in a series of solvents, as

shown in Figure S13a,b. DMSO, acetonitrile, and acetone are highly polar aprotic solvents with high dielectric constants of 46.7, 37.5, and 20.7, respectively, and they exhibit absorption maxima (λ_{max}) between 672–686 nm (Table S1). Among them, DMSO is a strong hydrogen bond acceptor (HBA), while acetonitrile and acetone are weak HBAs. The strong HBA nature of DMSO stabilizes the excited state of the dye and inhibits intermolecular interactions, promoting the monomeric form and resulting in a red-shifted λ_{max}. On the other hand, the weak HBA ability of acetonitrile and acetone facilitates the formation of H-aggregates, leading to hypsochromic shifts in the absorption spectrum. Furthermore, polar protic solvents such as 2-propanol, ethanol, and ethanol: water (1:1, v/v) can act as hydrogen bond donors, enhancing intermolecular interactions and promoting H-aggregate formation, thereby inducing further blue shift in absorption [18,19]. The fluorescence emission spectra also exhibited solvent-dependent behavior. The emission maximum was in the range of 684–710 nm, with the strongest fluorescence observed in aprotic solvents and significant quenching in protic solvents, especially ethanol: water (1:1, v/v) and 2-propanol. This quenching effect is likely due to increased non-radiative decay pathways caused by hydrogen bonding and dye aggregation. To quantitatively assess the effect of solvent polarity on the photophysical properties of **SQ-68**, a Lippert–Mataga plot (see SI Section S5) was constructed by plotting the Stokes shift of **SQ-68** against the orientation polarizability (Δf) of each solvent, as shown in Figure S14. A gradual increase in the Stokes shift with Δf was observed, indicating that the **SQ-68** exhibits positive solvatochromism. The Lippert–Mataga analysis also reveals the distinct solvatochromic behavior of **SQ-68** in polar protic and aprotic solvents [20].

The Stokes shift, which represents the difference between the absorption maximum and the emission maximum, was calculated to be 24 nm in acetonitrile and 40 nm in the ethanol: water (1:1, v/v) solvent system (Table 1). The relatively small Stokes shift in acetonitrile suggests minimal structural or electronic reorganization between the ground and excited states. The dye remains largely in its monomeric and planar conformation with limited rearrangement [21,22]. In contrast, the significantly larger Stokes shift observed in the ethanol: water (1:1, v/v) system reflects increased stabilization of the excited state, likely due to enhanced hydrogen bonding and polarity effects, as well as possible aggregate formation. The presence of water in the solvent mixture promotes H-aggregate formation, which alters the π-electron distribution and leads to significant changes in the excited-state properties, such as a blue-shifted absorption band [23,24].

3.2. Absorption Studies of **SQ-68** *Towards Various Metal Cations*

For the selective interaction of **SQ-68** with different metal ions, a 10 μM solution of **SQ-68** was treated with 10 eq. of different metal ions (Li^+, Na^+, K^+, Cs^+, Mg^{2+}, Ca^{2+}, Mg^{2+}, Zn^{2+}, Pb^{2+}, Ni^{2+}, Fe^{2+}, $Cr3^+$, Co^{2+}, Cd^{2+}, Al^{3+}, and Ag^+) in both the acetonitrile and ethanol: water (1:1, v/v) solvent systems. In acetonitrile, the blank **SQ-68** solution appeared vivid cyan, which was clearly visible to the naked eye. Upon addition of the various metal ions, only Cu^{2+} induced a distinct color change, turning the solution from cyan to colorless, indicating a strong and selective interaction, as shown in Figure 2a. This visual observation was supported by UV–vis absorption spectral observation, where the characteristic absorption peak of **SQ-68** at 672 nm, corresponding to its monomeric form, completely disappeared upon Cu^{2+} addition, and a new absorption band emerged at 503 nm, indicating a significant blue shift (Figure 2c). In contrast, with Al^{3+} and Cr^{3+}, a noticeable, blue-shifted absorption peak was observed, suggesting partial perturbation of the dye's electronic structure; however, no significant color change was observed. For all other metal ions tested, neither spectral nor visible color changes were observed under the same conditions. Interestingly, when the solvent system was switched to ethanol:

water (1:1, v/v), the selectivity of **SQ-68** changed markedly. In this solvent system, **SQ-68** displayed a pronounced and selective response to Ag^+ ions. The addition of 10 eq. of Ag^+ ion resulted in a clear color change from cyan to colorless, which was easily observed by the naked eye (Figure 2b). Correspondingly, the absorption band at 670 nm (Figure 2d) disappeared completely, while a new peak appeared at 532 nm. Importantly, none of the other tested metal ions induced significant changes in either the solution color or the absorption spectrum under these conditions. The complete disappearance of the 672 nm band and the appearance of a new band at 503 nm in the presence of Cu^{2+} in acetonitrile, as well as the disappearance of the 670 nm band and the emergence of a 532 nm band with Ag^+ in ethanol: water (1:1, v/v), indicate strong binding and electronic interactions between **SQ-68** and these metal ions, most likely due to the formation of stable **SQ-68**-Cu^{2+} and **SQ-68**-Ag^+ complexes. Similarly, the fluorescence spectra of **SQ-68** (10 μM) were measured in the presence of various metal ions in both acetonitrile and ethanol: water solvent systems, with excitation at 610 nm. In both solvents, **SQ-68** displayed strong fluorescence emission intensity around 700 nm Figure S15. When metal ions were introduced, significant differences in the fluorescence intensity in both solvents were observed. Specifically, Cu^{2+} ions caused almost complete quenching of fluorescence in the acetonitrile solvent, suggesting a strong interaction. In contrast, in the ethanol: water solvent system, Ag^+ ions induced a notable quenching effect on the fluorescence emission. These distinct quenching effects arise from the specific interactions between **SQ-68** and metal ions. This consistent selectivity across both absorption and fluorescence measurements highlights the **SQ-68**'s robust and specific interaction with Cu^{2+} and Ag^+.

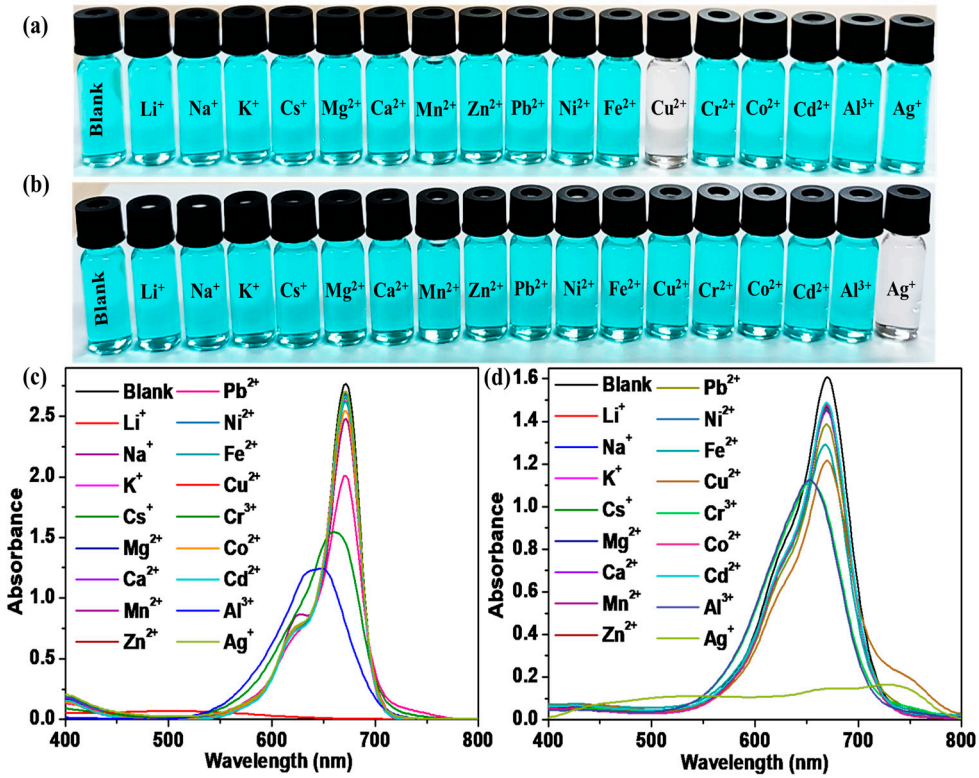


Figure 2. Colorimetric response of **SQ-68** in (**a**) acetonitrile and (**b**) ethanol: water (1:1, v/v). Absorption spectrum of 10 μM **SQ-68** in (**c**) acetonitrile and (**d**) ethanol: water (1:1, v/v) following addition of 10 eq. of various metal ions.

In acetonitrile, **SQ-68** showed a selective response to Cu^{2+}, whereas the ethanol: water (1:1, v/v) solvent system exhibited high selectivity for Ag^+, which suggests that the selectivity of **SQ-68** towards Cu^{2+} and Ag^+ could be controlled by switching solvent

media. Moreover, the results indicate that **SQ-68** displays solvent-dependent selectivity, allowing for the naked-eye detection of Cu^{2+} in acetonitrile and Ag^{+} in ethanol: water (1:1, *v*/*v*) through a clear color change from cyan to colorless, along with distinctive spectral shifts. This dual-mode response highlights the versatility of **SQ-68** as a practical and highly selective colorimetric probe for selective multiple ion detection.

3.3. Competition and Response Time Study of **SQ-68** *with* Cu^{2+} *and* Ag^{+}

To utilize **SQ-68** as an ion-selective chemosensor for Cu^{2+} and Ag^{+}, competitive experiments were conducted. To evaluate the selectivity of **SQ-68** for the detection of Cu^{2+} and Ag^{+} ions, absorption spectra were recorded for **SQ-68** (10 μM) in the presence of 10 eq. Cu^{2+} and Ag^{+} mixed with 10 eq. of other interfering metal ions (Li^{+}, Na^{+}, K^{+}, Cs^{+}, Mg^{2+}, Ca^{2+}, Mg^{2+}, Zn^{2+}, Pb^{2+}, Ni^{2+}, Fe^{2+}, Cr^{3+}, Co^{2+}, Cd^{2+}, Al^{3+}, and Ag^{+}). As illustrated in Figure 3a, the absorbance of **SQ-68** remained high when only interfering metal ions were present. However, upon the addition of Cu^{2+} or Ag^{+}, either alone or in combination with other metal ions, a pronounced decrease in absorbance was observed. This sharp change was not affected by the presence of other metal ions, clearly demonstrating the exceptional recognition specificity of **SQ-68** for Cu^{2+} and Ag^{+} ions. In the presence of other metal ions, **SQ-68** exhibits a λ_{max} at 672 nm and 670 nm (Figures S16a and S17a), and the solution retains its characteristic cyan color. Upon the addition of Cu^{2+} or Ag^{+} in acetonitrile and the ethanol: water (1:1, *v*/*v*) solvent system, a distinct blue shift is observed, with λ_{max} shifting to 503 nm and 532 nm (Figures S16b and S17b), respectively, corresponding to the formation of **SQ-68**-Cu^{2+} and **SQ-68**-Ag^{+} complexes. This spectral change is also visually apparent: while other metal ions do not alter the cyan color of the solution, only Cu^{2+} and Ag^{+} cause the solution to become colorless. Furthermore, when **SQ-68** is mixed with all metal ions, including Cu^{2+} or Ag^{+}, the absorption bands remain within the 400–550 nm range (Figures S16 and S17) due to complex formation, and the solution consistently appears colorless. These results suggest that **SQ-68** functions as a highly selective and reliable colorimetric sensor for Cu^{2+} and Ag^{+}. The results clearly showed that the interference of other metals with the absorption response of **SQ-68** could be ignored in the detection of Cu^{2+} and Ag^{+}. This outstanding selectivity and clear colorimetric response make **SQ-68** a promising candidate for the detection of Cu^{2+} and Ag^{+} in various real-world samples, such as water analysis, where complex ionic backgrounds are common.

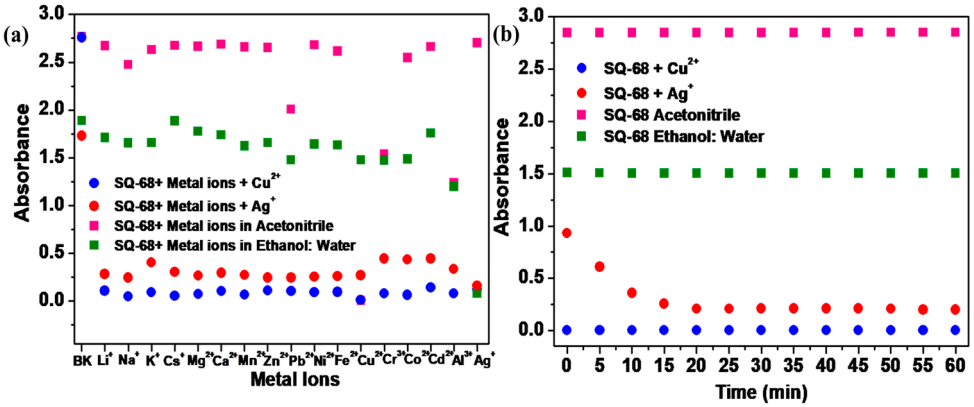


Figure 3. (**a**) The selectivity of **SQ-68** (10 μM) for Cu^{2+} and Ag^{+} in the presence of different metal ions and (**b**) the response of **SQ-68** (10 μM) in the presence of Cu^{2+} and Ag^{+}.

The response time of a sensor is a critical parameter that determines its practical utility for the rapid detection of target analytes. In this study, the absorption spectral behavior of **SQ-68** (10 μM) was systematically investigated upon its addition to 10 eq. of Cu^{2+} or Ag^{+} ions. As shown in Figure 3b, the absorbance of **SQ-68** at 672 nm (for Cu^{2+}) and 670 nm (for

Ag^+) showed no absorption change and remained stable over 60 min before the addition of metal ions, confirming **SQ-68**'s excellent stability in solution (Figures S18a and S19a). When Cu^{2+} was introduced, the absorbance at 672 nm rapidly and significantly decreased, dropping close to zero within approximately 2 min and remaining constant for the duration of the experiment (Figure S18b). This rapid spectral change indicates an ultra-fast and strong binding interaction between **SQ-68** and Cu^{2+} ions. Similarly, when Ag^+ ions were added, the absorbance at 670 nm also decreased significantly, reaching its minimum after 15 min and remaining stable within the tested time (Figure S19b). The consistent and stable low absorbance values following the initial response for both ions highlight the robustness and reliability of the sensor. Collectively, these results demonstrate that **SQ-68** can provide a rapid optical response to both Cu^{2+} and Ag^+ ions, with complete detection achieved within 2 min for Cu^{2+} and 15 min for Ag^+. Although both Cu^{2+} and Ag^+ form thermodynamically favorable complexes with the **SQ-68** probe, the Cu^{2+} complexes exhibit significantly faster binding kinetics. This difference can be attributed to a combination of interrelated factors. Cu^{2+} has a higher charge density and smaller ionic radius than Ag^+, leading to stronger electrostatic interactions due to higher Lewis acidity. Additionally, according to Pearson's hard and soft acids and bases (HSAB) theory, Cu^{2+} is classified as a borderline acid, making it well-matched to coordinate with borderline or hard bases such as nitrogen and oxygen. This favorable acid–base compatibility further enhances its binding efficiency and contributes to a lower energy activation barrier for complex formation. In contrast, Ag^+ is a soft acid, which preferentially binds to soft donor atoms. Since the **SQ-68** probe lacks such soft donor sites and primarily contains harder donor atoms, Ag^+ experiences a mismatch in HSAB compatibility. As a result, Ag^+ requires a longer time to form a stable complex with **SQ-68** [25–27]. Furthermore, time-dependent absorption at the λ_{max} was carried out to monitor changes in the absorbance of **SQ-68** as a function of time upon interaction with Cu^{2+} and Ag^+, which represents how quickly the probe responds to the metal ions, as depicted in Figure S20a,b. When the probe interacts with Cu^{2+} ions, it results in a rapid decrease in absorbance, a much higher rate of 0.17 s^{-1}, and a short response time of only 40 s, signifying a strong binding affinity along with faster complexation kinetics. In contrast, with Ag^+ ions, the decrease in absorbance is very gradual, with a slow rate of 0.0023 s^{-1} and a long response time of 7000 s, indicating a weak or slow binding process between the **SQ-68** and Ag^+ ions. This means **SQ-68** responds to Cu^{2+} ions 175 times faster than to Ag^+ ions, demonstrating a dramatically higher sensitivity and much quicker detection capability for Cu^{2+} ions.

To complement these experimental findings, density functional theory (DFT) calculations were carried out to gain insight into the kinetics and binding energy behavior of the synthesized **SQ-68** dye with Cu^{2+} and Ag^+ ions. All structural optimizations were carried out using the Gaussian 16 software package. The B3LYP functional with the LanL2DZ basis set was employed for geometry optimization, and all optimized structures were confirmed by vibrational frequency analysis to have no imaginary frequencies, ensuring that true minima were obtained. To simplify the interpretation of binding behavior and isolate the fundamental interaction mechanism, a model of **SQ-68** was considered in which the Cu^{2+} and Ag^+ ions coordinate to only one functional site, as illustrated in Figure 4. Interaction energies for complex formation were calculated using the free energy and enthalpy differences between the complexes and **SQ-68**. The calculated Gibbs free energy changes (ΔGs) for the formation of the **SQ-68**–Cu^{2+} and **SQ-68**–Ag^+ complexes were—400 kcal/mol and –77 kcal/mol, respectively. Similarly, the enthalpy changes (ΔHs) were found to be—410 kcal/mol for Cu^{2+} and—92 kcal/mol for Ag^+. These values indicate that the formation of the **SQ-68**–Cu^{2+} complex is significantly more thermodynamically fa-

vorable than that of the **SQ-68**–Ag^+ complex. Furthermore, the rate constant for the complex reactions was estimated using Equation (1), based on the calculated free energy changes.

$$\boldsymbol{k}(T) = \frac{K_B T}{hc^\circ} e^{-\Delta G^\circ / RT} \quad (1)$$

where k_B is the Boltzmann constant, T is the temperature, h is Planck's constant, ΔG° is the Gibbs free energy of activation, R is the gas constant, and k(T) is the reaction rate at temperature T. An examination of Equation (1) corroborates that the rate constant k(T) varies exponentially with $-\Delta G$. Since the ΔG of **SQ-68**–Cu^{2+} is almost 5 times higher than that of **SQ-68**–Ag^+, this translates to an approximately 145 times higher rate of complexation of **SQ-68** with Cu^{2+} compared to that of Ag^+ ions. This theoretical calculation also supports that the experimental response time for complexation with Ag^+ ion is approximately 175 times slower than that of its Cu^{2+} ion counterpart discussed before. Collectively, both experimental and theoretical results consistently demonstrate that **SQ-68** exhibits a much stronger and faster binding affinity toward Cu^{2+} compared to Ag^+.

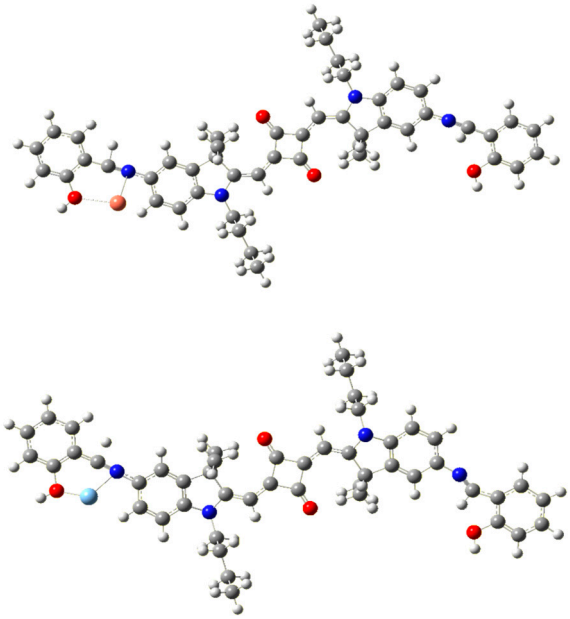


Figure 4. Optimized molecular structure of **SQ-68**-Cu^{2+} (**top**) and **SQ-68**-Ag^+ (**bottom**) obtained after quantum chemical MO calculations using Gaussian G16.

3.4. Sensing Mechanism of **SQ-68** *Response Toward* Cu^{2+} *and* Ag^+

To thoroughly investigate the sensing behavior and binding characteristics of **SQ-68** towards Cu^{2+} and Ag^+ ions, both a Job's plot and Benesi–Hildebrand analysis were performed in acetonitrile and ethanol: water (1:1, v/v) solvent systems [28,29]. For the Job's plot experiments, the solutions were prepared in which the total concentration of **SQ-68** and the metal ion (either Cu^{2+} or Ag^+) was maintained at 10 μM, while the mole fraction of the **SQ-68** to metal ion was systematically varied from 0 to 1. At each ratio, the absorbance was recorded at the characteristic's wavelength corresponding to the metal–ligand complex. The plots revealed a peak absorbance change at a mole fraction of 0.5 for both Cu^{2+} and Ag^+ (Figure 5a), clearly confirming the formation of a 1:1 complex between **SQ-68** and each metal ion. Upon the addition of Cu^{2+} or Ag^+ to the **SQ-68** solution, a pronounced and visually observable color change was noted, which corresponded to a distinct spectral shift in the absorption spectra (Figure S21a,b). In the metal-free state, **SQ-68** displays prominent absorption maxima at 672 nm and 670 nm, characteristics of its uncomplexed state. Upon the addition of Cu^{2+} ions, the absorption band at 672 nm rapidly

decreases in intensity, accompanied by the emergence of a new peak at 503 nm. Similarly, when Ag^+ ions are introduced, the original absorption maximum at 670 nm diminishes, and a new peak appears at 532 nm. These pronounced blue shifts in the absorption maxima are indicative of a ligand-to-metal charge transfer (LMCT) process, wherein electron density is transferred from the imine nitrogen and phenolic oxygen donor atoms of the **SQ-68** ligand to the vacant d-orbitals of the Cu^{2+} and Ag^+ ions [30–32]. This coordination leads to significant perturbations of the **SQ-68** electronic structure, resulting in the observed changes in the electronic absorption spectrum. The schematic representation of 1:1 **SQ-68**-Cu^{2+} and **SQ-68**-Ag^+ ion complex formation is shown in Figure 6.

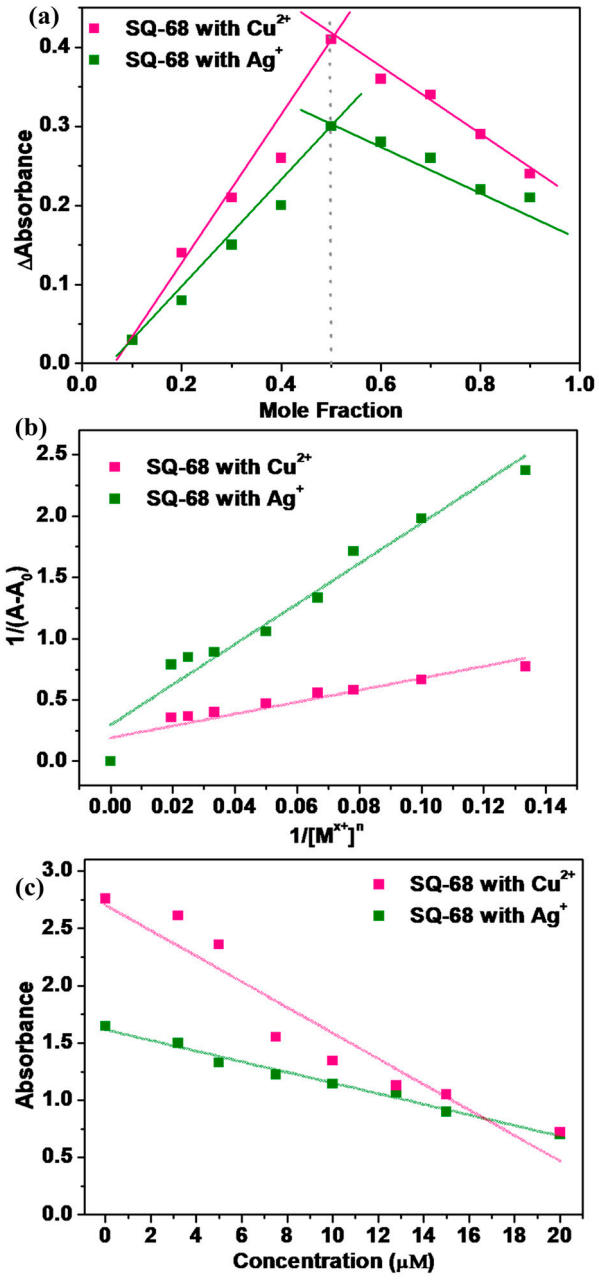


Figure 5. (**a**) Jobs plot illustrating the stoichiometry of the **SQ-68**-Cu^{2+} and **SQ-68**-Ag^+ complexes; (**b**) Benesi–Hildebrand plot at $1/(A - A_0)$ vs. $1/[M^{x+}]^n$ at a fixed probe concentration of 10 uM; (**c**) calibration curve for the absorption intensity of **SQ-68** towards the Cu^{2+} and Ag^+ concentrations.

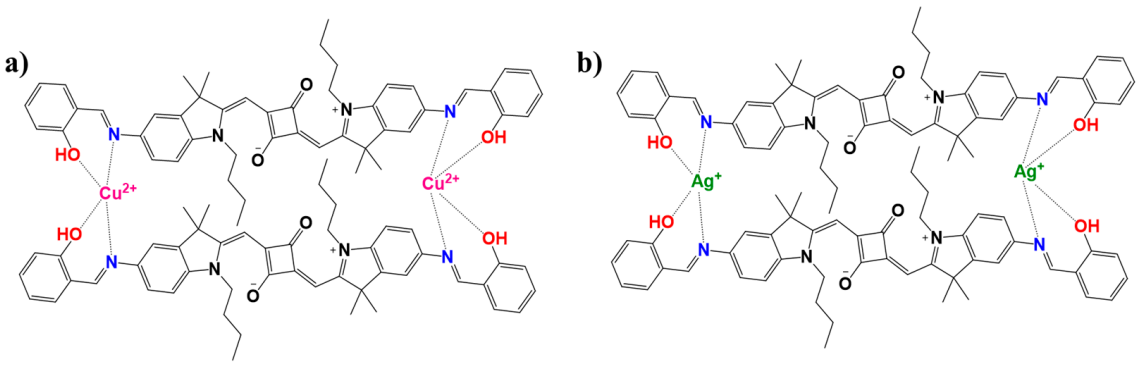


Figure 6. Schematic illustration depicting the plausible mechanism and binding modes of the **SQ-68** (**a**) Cu^{2+} and (**b**) Ag^{+} ions.

To further confirm the binding stoichiometry and quantify the interaction strength between **SQ-68** and the metal ions, a Bensei–Hildebrand (B–H) analysis was performed by maintaining a fixed **SQ-68** concentration (10 μM) while titrating Cu^{2+} or Ag^{+} (0–50 μM [33,34]. As shown in Figure S22a,b, increasing metal ion concentrations caused progressively decreasing absorption bands of **SQ-68** at 672 nm (Cu^{2+}) and 670 nm (Ag^{+}). The decrease in absorbance is attributed to the chelation of Cu^{2+} or Ag^{+} ions with the imine nitrogen and phenolic oxygen atoms of the **SQ-68** ligand, which disrupts the D-A-D charge transfer pathway within the molecule and results in quenching of the original absorption band [35]. The binding constant (k_a) was determined using the (B–H) Equation (2).

$$\frac{1}{A - A_0} = \frac{1}{k_a(A_{max} - A_0)[M^{x+}]^n} + \frac{1}{A_{max} - A_0} \quad (2)$$

where 'A' is the absorbance in the presence of Cu^{2+} or Ag^{+} ion, 'A_0' represents the absorbance of the ligand in the absence of Cu^{2+} or Ag^{+}, and 'A_{max}' corresponds to the absorbance at the absorption maximum. The k_a was determined from the slope of the linear plot of $1/(A - A_0)$ versus $1/[M^{x+}]^n$, where M^{n+} represents the metal ions (Cu^{2+} or Ag^{+}) (Figure 5b). The plot exhibited a linear relationship when n = 1, confirming a 1:1 binding stoichiometry between **SQ-68** and both metal ions. The k_a values, calculated from the slopes of these plots, were found to be 2.05×10^5 M^{-1} for Cu^{2+} and 6.06×10^4 M^{-1} for Ag^{+}, indicating strong binding affinity and highly stable complex formation. To further understand the thermodynamics of these interactions, the Gibbs free energy change (**ΔG**) was calculated using the relationship $\Delta G = -RTlnk_a$, where R is the gas constant and T is absolute temperature. The resulting ΔG value of -30.3 $kJmol^{-1}$ for the **SQ-68**-Cu^{2+} complex and -27.3 $kJmol^{-1}$ for the **SQ-68**-Ag^{+} complex indicates that the formation of both complexes is highly favorable and occurs spontaneously.

The Fourier transform infrared (FTIR) spectroscopic analysis was carried out for the **SQ-68**-Cu^{2+} and **SQ-68**-Ag^{+} complexes, as shown in Figure S23. Upon complexation, notable shifts in both the position and intensity of absorption bands were observed, revealing important details about the binding interactions of **SQ-68**. In the free **SQ-68**, a strong and sharp absorption band at 1590 cm^{-1} corresponds to the ν(C=N) stretching vibration, which is characteristic of the imine functionalities present in the ligand. Upon complexation with either Cu^{2+} or Ag^{+}, this band shifts to a lower wavenumber 1580 cm^{-1} (Cu^{2+}) and 1565 cm^{-1} (Ag^{+}), indicating a weakening of the C=N bond due to electron donation from the imine nitrogen to the metal center. This shift is accompanied by a broadening and a decrease in the intensity of the band, which are characteristics of coordination to transition metal ions. Additionally, the phenolic C-O stretching vibration, which appears at 1260 cm^{-1} in the free probe, shifts to around 1270 cm^{-1} for the Cu^{2+} and 1271 cm^{-1} for the

Ag^+ complexes. This result suggested that the nitrogen and oxygen atoms in the **SQ-68** moiety participated in the coordination with Cu^{2+} and Ag^+ [36–38].

In addition to binding strength, the analytical performance of **SQ-68** as a colorimetric sensor was evaluated by constructing calibration curves for Cu^{2+} and Ag^+. A strong linear relationship was observed when plotting peak absorbance against metal ion concentration, indicating its suitability for quantitative analysis (Figure 5c). The sensitivity (k), limit of detection (LOD), and limit of quantification (LOQ) are important performance parameter matrices of a sensing probe, which are most widely estimated using Equations (3)–(5).

$$Sensitivity = k \tag{3}$$

$$LOD = \frac{3\sigma}{k} \tag{4}$$

$$LOQ = \frac{10\sigma}{k} \tag{5}$$

The sensitivity of **SQ-68** toward Cu^{2+} and Ag^+ ions was evaluated using the slope of the calibration curves (Equation (2) and Figure 5c), resulting in values of 1.12×10^{-1} for Cu^{2+} and 4.64×10^{-2} uM^{-1} for Ag^+. The analytical performance was further evaluated by determining the LOD and LOQ, calculated using conventional equations (Equations (4) and (5)), where 'σ' denotes the standard deviation of the blank solution and '*k*' corresponds to the slope of the calibration curve (Figure 5c) [39,40]. Substitutions of the corresponding values of the LOD and LOQ for Cu^{2+} were determined to be 0.09 μM and 0.31 μM, respectively, while for Ag^+, they were 0.38 μM and 1.26 μM. Notably, these detection limits are lower than the maximum allowable concentrations for Cu^{2+} (1.3 mg/L) and Ag^+ (0.1 mg/L) in drinking water, as set by the USEPA and WHO [41]. Such low LOD and LOQ values highlight the excellent sensitivity and selectivity of **SQ-68** as a colorimetric sensor for Cu^{2+} and Ag^+ ions, making it highly suitable for trace-level detection in environmental applications.

The development of **SQ-68** as an optical absorption-based colorimetric probe in the acetonitrile and ethanol: water (1:1, *v*/*v*) mediums provides a selective and sensitive approach for Cu^{2+} and Ag^+ detection. To assess the superior performance of **SQ-68** compared to previously reported Cu^{2+} and Ag^+ chemosensors, a comparative analysis was performed and is presented in Table 2, which summarizes the different Cu^{2+} and Ag^+ sensors along with their respective solvent systems, sensing methods, binding stoichiometry, and LOD values. This comparison highlights that **SQ-68** offers several distinctive advantages over previously reported systems, including instantaneous naked-eye detection, a significantly lower detection limit, a faster response time, and operational simplicity, making it an ideal candidate for real-time Cu^{2+} and Ag^+ sensing applications.

Table 2. Comparison of previously reported probes for the detection of Cu^{2+} and Ag^+ ions.

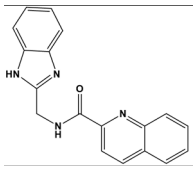
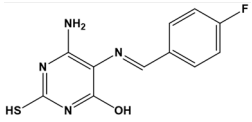
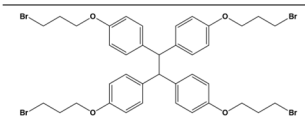
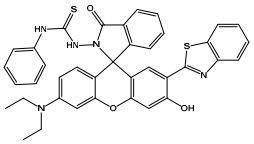
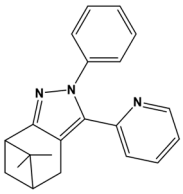
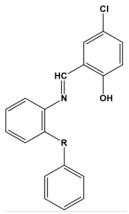
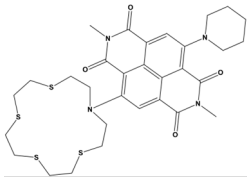
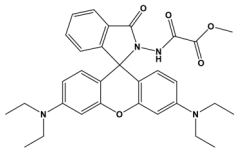
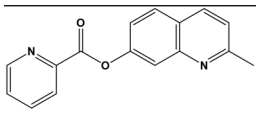
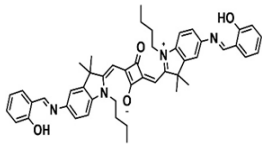
Probe	Probe Name	Solvent System	Sensing Method	LOD (μM)	Ref.
	L	MeOH/Tris buffer (1:1, *v*/*v*)	Fluorescent sensor	0.44 Ag^+	[42]
	5-(-4-fluorobenzylideneamino)-6-amino-2-mercaptopyrimidin-4-ol	DMF/HEPES buffer (1:1, *v*/*v*)	Colorimetric and Fluorescent sensor	1.12 Ag^+	[43]

Table 2. *Cont.*

Probe	Probe Name	Solvent System	Sensing Method	LOD (μM)	Ref.
	TPE-4DDC	H_2O/THF	Fluorescent sensor	0.87 Ag^+	[44]
	RBTP	H_2O/THF	Fluorescent sensor	0.45 Ag^+	[45]
	PPN	DMF/PBS	Colorimetric sensor	0.86 Ag^+ 0.56 Cu^{2+}	[46]
	Probe 1 and Probe 2	DMSO/PBS buffer	Colorimetric and Fluorescent sensor	0.22 and 0.72 Cu^{2+}	[47]
	NDI-4	CH_3CN	Fluorescent sensor	4.0 Cu^{2+}	[48]
	1	HEPES buffer/CH_3CN (40:60, *v*/*v*)	Fluorescent sensor	0.95 Cu^{2+}	[49]
	Probe PQ	HEPES buffer	Fluorescent sensor	0.15 Cu^{2+}	[50]
	**SQ-68**	**CH_3CN Ethanol: Water (1:1, *v*/*v*)**	**Colorimetric Sensor**	**0.38 Ag^+ 0.09 Cu^{2+}**	**Our work**

3.5. Application to Environmental Water Samples

To demonstrate the practical applicability of the **SQ-68** sensor for trace metal ion detection, we evaluated its performance in real environment water samples, including seawater, lake water, and tap water [51,52]. In addition, to ensure the practical applicability of **SQ-68**, we evaluated its performance under various pH conditions (pH 4, 7, and 12). Since the absorption properties of **SQ-68** for detecting Cu^{2+} and Ag^+ ions could potentially be influenced by pH, we systematically investigated its absorption responses at these pH values using UV–vis spectroscopy in the presence of respective metal ions. As shown in Figure S24a,b, which present the absorbance spectra of **SQ-68** upon interaction with metal ions, the main absorption bands remain largely unchanged across the entire pH

range, indicating that **SQ-68** can reliably detect Cu^{2+} and Ag^{+} ions over a broad pH range, highlighting its suitability for practical applications.

Each sample was first filtered through a 0.22 µm Rephiquik syringe filter to remove insoluble impurities, ensuring a clear medium for analysis. Subsequently, the samples were spiked with known concentrations of Cu^{2+} and Ag^{+} ions at levels of 5, 10, 20, and 40 µM to assess the sensor's ability to accurately quantify target analytes in complex aqueous environments (Figures 7a,b, S25 and S26). The absorption spectra of these spiked samples were recorded, revealing that the **SQ-68** sensor exhibited high recovery rates across all tested water types. The highest recoveries were observed in seawater, with 96% for Cu^{2+} and 99% for Ag^{+}, while the lowest recoveries appeared in lake water, with 73% for Cu^{2+} and 59% for Ag^{+} (Tables S2 and S3). These variations are likely attributable to matrix effects and the diverse ionic composition of the different water sources, which can influence sensor performance through competitive binding. Notably, the absorbance data displayed a consistent decrease with increasing metal ion concentrations, confirming the sensor's reliable response and minimal interference from coexisting species. These results confirmed that probe **SQ-68** has strong potential in environmental monitoring, as it exhibits the precise and reproducible detection of Cu^{2+} and Ag^{+} ions even in the presence of complex sample matrices.

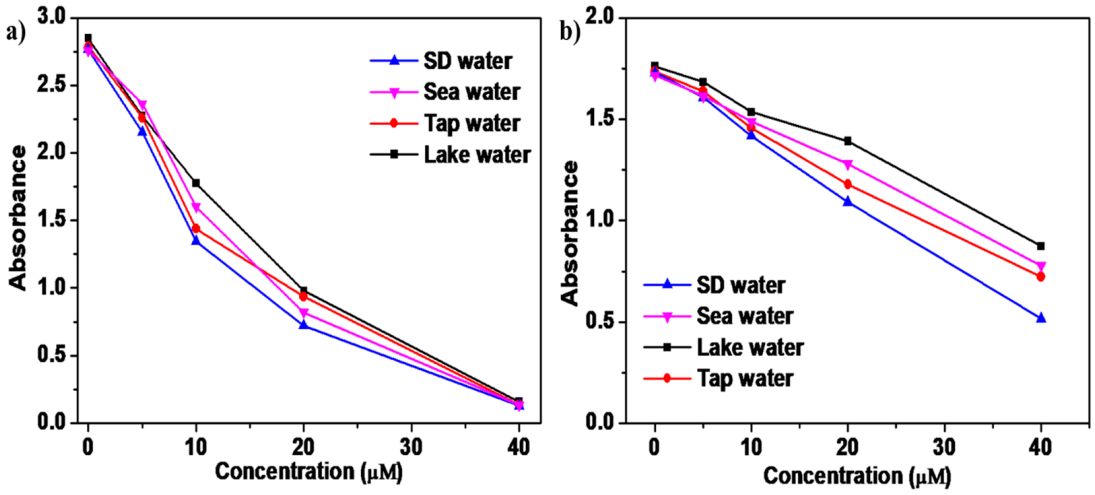


Figure 7. (**a**) Real-world sample analysis using **SQ-68** for determining Cu^{2+} and (**b**) Ag^{+} in seawater, lake water, and tap water.

4. Conclusions

In conclusion, a symmetrical squaraine-dye-based novel probe **SQ-68** was successfully synthesized and characterized. Importantly, **SQ-68** exhibited a unique dual-ion detection capability, where it showed high selectivity for Cu^{2+} in acetonitrile and for Ag^{+} in the ethanol: water (1:1, v/v) solvent system. **SQ-68** showed strong affinity towards these metal ions, with a binding constant of 2.05×10^{5} M^{-1} for Cu^{2+} and 6.06×10^{4} M^{-1} for Ag^{+}. The Job's plot and Benesi–Hilderbrand analyses confirmed a 1:1 binding stoichiometry between **SQ-68** and each metal ion, while FTIR spectroscopy provided further evidence for complex formation, as indicated by characteristic shifts in the C=N stretching vibration upon coordination. Moreover, **SQ-68** achieved a very low limit of detection of 0.09 µM for Cu^{2+} and 0.38 µM for Ag^{+}, making it a highly effective colorimetric chemosensor. The rapid response of the newly designed probe and excellent specificity make it highly suitable for real-time monitoring of Cu^{2+} and Ag^{+} contamination in water sources. Notably, **SQ-68** enabled the detection of metal ion concentrations well below the permissible limits set by the USEPA, highlighting its practical utility for environmental safety.

Supplementary Materials: The following supporting information can be downloaded at https://www.mdpi.com/article/10.3390/chemosensors13080288/s1: Scheme S1. Synthetic scheme of **SQ-68**. Figure S1: HR-MS spectrum of (1); Figure S2: HR-MS spectrum of (2); Figure S3: HR-MS spectrum of (3); Figure S4: TOF-MS spectrum of (4); Figure S5: TOF-MS spectrum of (5); Figure S6: TOF-MS spectrum of (6); Figure S7: ^{1}H NMR spectra of compound (1); Figure S8: ^{1}H NMR spectra of compound (2); Figure S9: ^{1}H NMR spectra of compound (3); Figure S10: ^{1}H NMR spectra of compound (4); Figure S11: ^{1}H NMR spectra of compound (5); Figure S12: ^{1}H NMR spectra of compound **SQ-68**; Figure S13: (a) Electronic absorption and (b) fluorescence emission spectra (λex = 610 nm, excitation and emission bandwidths are 5 and 6, respectively) of **SQ-68** (10 μM) in different solvent systems; Figure S14: Lippert–Mataga correlation between Stokes shift and orientation polarizability for **SQ-68** (10 μM); Figure S15: Fluorescence spectra of **SQ-68** (10 μM) with various metal ions in (a) acetonitrile (λex = 610 nm, excitation and emission bandwidths are 5 and 6, respectively) and (b) ethanol: water (λex = 610 nm, excitation and emission bandwidths are 5 and 10, respectively) solvent systems; Figure S16: (a) Absorption spectra of **SQ-68** (10 μM) in acetonitrile solvent upon addition of 10 eq. of various metal ions; (b) absorption spectra of **SQ-68** (10 μM) for Cu^{2+} in presence of other metal ions; Figure S17: (a) Absorption spectra of **SQ-68** (10 μM) in ethanol: water (1:1, *v*/*v*) solvent upon addition of 10 eq. of various metal ions; (b) absorption spectra of **SQ-68** (10 μM) for Ag^+ in presence of other metal ions; Figure S18: (a) Absorption spectra of **SQ-68** (10 μM) in acetonitrile with time; (b) absorption spectra of **SQ**-**68** (10 μM) with time in presence Cu^{2+}; Figure S19: Absorption spectra of **SQ-68** (10 μM) in ethanol: water (1:1, *v*/*v*) with time; (b) absorption spectra of **SQ-68** (10 μM) with time in presence of Ag^+; Figure S20: Kinetic study of **SQ-68**-Cu^{2+} and **SQ-68**-Ag^+; Figure S21: Electronic absorption spectra for (a) **SQ-68**-Cu^{2+} and (b) **SQ-68**-Ag^+ system with varying **SQ-68** mole fraction (1 to 0); Figure S22: Electronic absorption spectra of **SQ-68** (10 μM) in (a) CH_3CN with increasing concentration of Cu^{2+} and (b) EtOH: H_2O (1:1, *v*/*v*) upon incremental addition of Ag^+; Figure S23: Experimental FTIR spectra; Figure S24: Electronic absorption spectra of (a) **SQ-68**-Cu^{2+} and (b) **SQ-68**-Ag^+ at different pH (normalized); Figure S25: UV–visible spectra of real-world sample analysis of **SQ-68** (10 μM) in acetonitrile solvent: (a) SD, (b) sea, (c) lake, and (d) tap water; Figure S26: UV–visible spectra of real-world sample analysis of **SQ-68** in ethanol: water (1:1, *v*/*v*) solvent: (a) SD, (b) sea, (c) lake, and (d) tap water; Table S1: Optical characterization of **SQ-68** in various solvent systems; Table S2: Detection of Cu^{2+} in real-world samples; Table S3: Detection of Ag^+ in real-world samples.

Author Contributions: S.T. contributed to Data curation, Validation, Visualization, Investigation, and Writing the original draft. K.R.S. contributed to Validation, Visualization, Investigation, and Writing the original draft. S.S.P. contributed to Resources, Conceptualization, Validation, Project administration, Supervision, and Reviewing and editing of the manuscript draft. All authors have read and agreed to the published version of the manuscript.

Funding: This research received no external funding.

Institutional Review Board Statement: Not applicable.

Informed Consent Statement: Not applicable.

Data Availability Statement: All of the data used in this work are provided and presented in the main manuscript and the Supplementary Information (SI).

Acknowledgments: All of the authors are thankful to their respective affiliated institutes for supporting them throughout this work. K.R.S. would like to thank the Ministry of Education, Culture, Sports, and Science (MEXT), Japan, for providing the scholarship under the PhD program.

Conflicts of Interest: The funders had no role in the design of the study; in the collection, analysis, or interpretation of the data; in the writing of the manuscript; or in the decision to publish the results.

Abbreviations

The following abbreviations are used in this manuscript:

NIR	Near-infrared
USEPA	United States Environmental Protection Agency
TLC	Thin layer Chromatography
Fmoc-Osu	N-(9-Fluorenylmethoxycarbonyloxy) succinimide
MeOH	Methanol
CH_3CN	Acetonitrile
CH_3Cl	Chloroform
EtOH	Ethanol

References

1. Hu, L.; Yan, Z.; Xu, H. Advances in synthesis and application of near-infrared absorbing squaraine dyes. *RSC Adv.* **2013**, *3*, 7667. [CrossRef]
2. Ros-Lis, J.V.; Martínez-Máñez, R.; Sancenón, F.; Soto, J.; Spieles, M.; Rurack, K. Squaraines as Reporter Units: Insights into their Photophysics, Protonation, and Metal-Ion Coordination Behaviour. *Chem. A Eur. J.* **2008**, *14*, 10101–10114. [CrossRef] [PubMed]
3. Ananda Rao, B.; Kim, H.; Son, Y.-A. Synthesis of near-infrared absorbing pyrylium-squaraine dye for selective detection of Hg^{2+}. *Sens. Actuators B Chem.* **2013**, *188*, 847–856. [CrossRef]
4. Dey, N.; Kulhánek, J.; Bureš, F.; Bhattacharya, S. Simultaneous Detection of Cu^{2+} and Hg^{2+} via Two Mutually Independent Sensing Pathways of Biimidazole Push–Pull Dye. *J. Org. Chem.* **2019**, *84*, 1787–1796. [CrossRef]
5. Kim, H.N.; Ren, W.X.; Kim, J.S.; Yoon, J. Fluorescent and colorimetric sensors for detection of lead, cadmium, and mercury ions. *Chem. Soc. Rev.* **2012**, *41*, 3210–3244. [CrossRef]
6. Yamanaka, M.; Hara, K.; Kudo, J. Bactericidal Actions of a Silver Ion Solution on *Escherichia coli*, Studied by Energy-Filtering Transmission Electron Microscopy and Proteomic Analysis. *Appl. Environ. Microbiol.* **2005**, *71*, 7589–7593. [CrossRef]
7. Valko, M.; Morris, H.; Cronin, M. Metals, Toxicity and Oxidative Stress. *Curr. Med. Chem.* **2005**, *12*, 1161–1208. [CrossRef] [PubMed]
8. Barceloux, D.G.; Barceloux, D. Copper. *J. Toxicol. Clin. Toxicol.* **1999**, *37*, 217–230. [CrossRef]
9. Yao, J.; Zhang, K.; Zhu, H.; Ma, F.; Sun, M.; Yu, H.; Sun, J.; Wang, S. Efficient Ratiometric Fluorescence Probe Based on Dual-Emission Quantum Dots Hybrid for On-Site Determination of Copper Ions. *Anal. Chem.* **2013**, *85*, 6461–6468. [CrossRef] [PubMed]
10. Velmurugan, K.; Raman, A.; Easwaramoorthi, S.; Nandhakumar, R. Pyrene pyridine-conjugate as Ag selective fluorescent chemosensor. *RSC Adv.* **2014**, *4*, 35284–35289. [CrossRef]
11. Zhang, J.F.; Zhou, Y.; Yoon, J.; Kim, J.S. Recent progress in fluorescent and colorimetric chemosensors for detection of precious metal ions (silver, gold and platinum ions). *Chem. Soc. Rev.* **2011**, *40*, 3416. [CrossRef] [PubMed]
12. Shum, S.C.K.; Pang, H.M.; Houk, R.S. Speciation of mercury and lead compounds by microbore column liquid chromatography-inductively coupled plasma mass spectrometry with direct injection nebulization. *Anal. Chem.* **1992**, *64*, 2444–2450. [CrossRef]
13. Anderson, J.L.; Bowden, E.F.; Pickup, P.G. Dynamic Electrochemistry: Methodology and Application. *Anal. Chem.* **1996**, *68*, 379–444. [CrossRef]
14. Katarina, R.K.; Takayanagi, T.; Oshima, M.; Motomizu, S. Synthesis of a chitosan-based chelating resin and its application to the selective concentration and ultratrace determination of silver in environmental water samples. *Anal. Chim. Acta* **2006**, *558*, 246–253. [CrossRef]
15. Gupta, S.; Yamawaki, Y.; Pradhan, S.; Pandey, S.S.; Kato, T. Design and Synthesis of Novel Squaraine Dye with Highly Enhanced Far-Red Fluorescence and its Interaction with a Model Protein. *Phys. Status Solidi* **2023**, *220*, 2300226. [CrossRef]
16. McKerrow, A.J.; Buncel, E.; Kazmaier, P.M. Aggregation of squaraine dyes: Structure–property relationships and solvent effects. *Can. J. Chem.* **1995**, *73*, 1605–1615. [CrossRef]
17. De Feyter, S.; De Schryver, F.C. Two-dimensional supramolecular self-assembly probed by scanning tunneling microscopy. *Chem. Soc. Rev.* **2003**, *32*, 139–150. [CrossRef]
18. Priyanka; Bila, G.; Mavileti, S.K.; Bila, E.; Negrych, N.; Gupta, S.; Tang, L.; Bilyy, R.; Pandey, S.S.; Kato, T. A biocompatible NIR squaraine dye and dye-antibody conjugates for versatile long-term in vivo fluorescence bioimaging. *Mater. Adv.* **2024**, *5*, 3940–3949. [CrossRef]
19. Tang, L.; Sharma, S.; Pandey, S.S. Synthesis and Characterization of Newly Designed and Highly Solvatochromic Double Squaraine Dye for Sensitive and Selective Recognition towards Cu^{2+}. *Molecules* **2022**, *27*, 6578. [CrossRef]

20. Patra, D.; Barakat, C. Synchronous fluorescence spectroscopic study of solvatochromic curcumin dye. *Spectrochim. Acta Part A Mol. Biomol. Spectrosc.* **2011**, *79*, 1034–1041. [CrossRef]
21. Egorov, V.V. Quantum-classical mechanics: Luminescence spectra in polymethine dyes and J-aggregates. Nature of the small Stokes shift. *Results Phys.* **2019**, *13*, 102252. [CrossRef]
22. Paternò, G.M.; Moretti, L.; Barker, A.J.; D'Andrea, C.; Luzio, A.; Barbero, N.; Galliano, S.; Barolo, C.; Lanzani, G.; Scotognella, F. Near-infrared emitting single squaraine dye aggregates with large Stokes shifts. *J. Mater. Chem. C* **2017**, *5*, 7732–7738. [CrossRef]
23. Peyratout, C.; Daehne, L. Aggregation of thiacyanine derivatives on polyelectrolytes. *Phys. Chem. Chem. Phys.* **2002**, *4*, 3032–3039. [CrossRef]
24. Herz, A.H. Aggregation of sensitizing dyes in solution and their adsorption onto silver halides. *Adv. Colloid Interface Sci.* **1977**, *8*, 237–298. [CrossRef]
25. Huang, S.; Du, P.; Min, C.; Liao, Y.; Sun, H.; Jiang, Y. Poly(1-amino-5-chloroanthraquinone): Highly Selective and Ultrasensitive Fluorescent Chemosensor For Ferric Ion. *J. Fluoresc.* **2013**, *23*, 621–627. [CrossRef]
26. Pearson, R.G. Hard and soft acids and bases, HSAB, part 1: Fundamental principles. *J. Chem. Educ.* **1968**, *45*, 581. [CrossRef]
27. Lotfi, B.; Tarlani, A.; Akbari-Moghaddam, P.; Mirza-Aghayan, M.; Peyghan, A.A.; Muzart, J.; Zadmard, R. Multivalent calix[4]arene-based fluorescent sensor for detecting silver ions in aqueous media and physiological environment. *Biosens. Bioelectron.* **2017**, *90*, 290–297. [CrossRef]
28. Olson, E.J.; Bühlmann, P. Getting More out of a Job Plot: Determination of Reactant to Product Stoichiometry in Cases of Displacement Reactions and n:n Complex Formation. *J. Org. Chem.* **2011**, *76*, 8406–8412. [CrossRef]
29. Kuntz, I.D.; Gasparro, F.P.; Johnston, M.D.; Taylor, R.P. Molecular interactions and the Benesi-Hildebrand equation. *J. Am. Chem. Soc.* **1968**, *90*, 4778–4781. [CrossRef]
30. Chopra, T.; Sasan, S.; Devi, L.; Parkesh, R.; Kapoor, K.K. A comprehensive review on recent advances in copper sensors. *Coord. Chem. Rev.* **2022**, *470*, 214704. [CrossRef]
31. Li, M.; Sheth, S.; Xu, Y.; Song, Q. Ru(II)-bipyridine complex as a highly sensitive luminescent probe for Cu^{2+} detection and cell imaging. *Microchem. J.* **2020**, *156*, 104848. [CrossRef]
32. Sahu, M.; Kumar Manna, A.; Rout, K.; Mondal, J.; Patra, G.K. A highly selective thiosemicarbazone based Schiff base chemosensor for colorimetric detection of Cu^{2+} and Ag^{+} ions and turn-on fluorometric detection of Ag^{+} ions. *Inorganica Chim. Acta* **2020**, *508*, 119633. [CrossRef]
33. Li, Q.; Guo, Y.; Shao, S. A BODIPY based fluorescent chemosensor for Cu(II) ions and homocysteine/cysteine. *Sensors Actuators B Chem.* **2012**, *171–172*, 872–877. [CrossRef]
34. Aich, K.; Goswami, S.; Das, S.; Das Mukhopadhyay, C. A new ICT and CHEF based visible light excitable fluorescent probe easily detects in vivo Zn^{2+}. *RSC Adv.* **2015**, *5*, 31189–31194. [CrossRef]
35. Fan, J.; Chen, C.; Lin, Q.; Fu, N. A fluorescent probe for the dual-channel detection of Hg^{2+}/Ag^{+} and its Hg^{2+}-based complex for detection of mercapto biomolecules with a tunable measuring range. *Sens. Actuators B Chem.* **2012**, *173*, 874–881. [CrossRef]
36. Hiremath, K.B.; Shivashankar, M. A selective fluorescence chemosensor: Thiosemicarbazide Schiff base derivative for detection of Ag^{+} ions in living cells. *J. Mol. Struct.* **2024**, *1302*, 137490. [CrossRef]
37. Ara Elachi, K. Synthesis, Spectral and Thermal Characterization of Cu(II) Complexes Containing Schiff Base Ligands and Their Antibacterial Activity Study. *Am. J. Mater. Synth. Process.* **2019**, *4*, 43. [CrossRef]
38. Şenol, C.; Hayvali, Z.; Dal, H.; Hökelek, T. Syntheses, characterizations and structures of NO donor Schiff base ligands and nickel(II) and copper(II) complexes. *J. Mol. Struct.* **2011**, *997*, 53–59. [CrossRef]
39. Uhrovčík, J. Strategy for determination of LOD and LOQ values–Some basic aspects. *Talanta* **2014**, *119*, 178–180. [CrossRef]
40. Armbruster, D.A.; Pry, T. Limit of blank, limit of detection and limit of quantitation. *Clin. Biochem. Rev.* **2008**, *29* (Suppl. 1), S49–S52.
41. Li, L.-Q.; Gao, L.-J. A novel rosamine based fluorescent sensor for Ag^{+} recognition. *Spectrochim. Acta Part A Mol. Biomol. Spectrosc.* **2016**, *152*, 426–430. [CrossRef]
42. Chen, C.; Liu, H.; Zhang, B.; Wang, Y.; Cai, K.; Tan, Y.; Gao, C.; Liu, H.; Tan, C.; Jiang, Y. A simple benzimidazole quinoline-conjugate fluorescent chemosensor for highly selective detection of Ag^{+}. *Tetrahedron* **2016**, *72*, 3980–3985. [CrossRef]
43. Maurya, N.; Bhardwaj, S.; Singh, A.K. Selective colorimetric and fluorescence 'turn-on' sensor for Ag^{+} and in-situ sensing of CN^{-} (off–on-off) via displacement approach. *Mater. Sci. Eng. C* **2017**, *74*, 55–61. [CrossRef]
44. Li, Y.; Yu, H.; Shao, G.; Gan, F. A tetraphenylethylene-based "turn on" fluorescent sensor for the rapid detection of Ag^{+} ions with high selectivity. *J. Photochem. Photobiol. A Chem.* **2015**, *301*, 14–19. [CrossRef]
45. Chen, S.; Wang, W.; Yan, M.; Tu, Q.; Chen, S.-W.; Li, T.; Yuan, M.-S.; Wang, J. 2-Hydroxy benzothiazole modified rhodol: Aggregation-induced emission and dual-channel fluorescence sensing of Hg^{2+} and Ag^{+} ions. *Sens. Actuators B Chem.* **2018**, *255*, 2086–2094. [CrossRef]
46. Jiang, Q.; Wang, Z.; Li, M.; Song, J.; Yang, Y.; Xu, X.; Xu, H.; Wang, S. A nopinone based multi-functional probe for colorimetric detection of Cu^{2+} and ratiometric detection of Ag^{+}. *Photochem. Photobiol. Sci.* **2020**, *19*, 49–55. [CrossRef] [PubMed]

47. Gujuluva Gangatharan, V.K.; Mookkandi Palsamy, K.; Gandhi, S.; Jamespandi, A.; Kandasamy, A.; Arunachalam, T.; Shenmuganarayanan, A.; Balasubramaniyam, S.; Jegathalaprathaban, R. Reversible NIR fluorescent probes for Cu^{2+} ions detection and its living cell imaging. *Sens. Actuators B Chem.* **2018**, *255*, 3235–3247. [CrossRef]
48. Zong, L.; Song, Y.; Li, Q.; Li, Z. A "turn-on" fluorescence probe towards copper ions based on core-substitued naphthalene diimide. *Sens. Actuators B Chem.* **2016**, *226*, 239–244. [CrossRef]
49. Yoon, J.W.; Chang, M.J.; Hong, S.; Lee, M.H. A fluorescent probe for copper and hypochlorite based on rhodamine hydrazide framework. *Tetrahedron Lett.* **2017**, *58*, 3887–3893. [CrossRef]
50. Wang, J.; Zong, Q. A new turn-on fluorescent probe for the detection of copper ion in neat aqueous solution. *Sens. Actuators B Chem.* **2015**, *216*, 572–577. [CrossRef]
51. Granado-Castro, M.D.; Díaz-de-Alba, M.; Chinchilla-Real, I.; Galindo-Riaño, M.D.; García-Vargas, M.; Casanueva-Marenco, M.J. Coupling liquid membrane and flow-injection technique as an analytical strategy for copper analysis in saline water. *Talanta* **2019**, *192*, 374–379. [CrossRef] [PubMed]
52. Kitte, S.A.; Li, S.; Nsabimana, A.; Gao, W.; Lai, J.; Liu, Z.; Xu, G. Stainless steel electrode for simultaneous stripping analysis of Cd(II), Pb(II), Cu(II) and Hg(II). *Talanta* **2019**, *191*, 485–490. [CrossRef] [PubMed]

Disclaimer/Publisher's Note: The statements, opinions and data contained in all publications are solely those of the individual author(s) and contributor(s) and not of MDPI and/or the editor(s). MDPI and/or the editor(s) disclaim responsibility for any injury to people or property resulting from any ideas, methods, instructions or products referred to in the content.